6.8.5 Cavity Safety and Environmental Impact

6.8.5.1 Introduction – The primary goal associated with cavity safety is to design a cavity which is inherently safe. The adopted design elementsinclude: (1) selection of materials which are inherently low activation, (2) minimization of corrosion and chemical interactions, (3) promotion of tritium release, and (4) minimization and control of tritium permeation. Safety concerns include source term characterization (or activation products) and accident tolerance in the cavity. Table 6.8.5-1 lists the possible failure modes which might occur in the cavity and their associated consequences. The safety hazards posed by activation products are the potential off-site dose if those isotopes are released to the environment and the decay heat available to damage structures if cooling is inadequate.

Radioactive materials existing in the cavity are: (1) tritium; (2) activated debris from burned pellets; (3) activated structural and shielding material in the first wall, blanket, reflector, and radiation shield; and (4) activated coolant.

Tritium inventory within the blanket is estimated at less than 100 grams. Permeation of tritium from the coolant into the steam cycle is a safety concern. Helium and lead are two major heat transfer media in the reactor designs. A major portion of the thermal energy is transferred with the helium coolant which has a low solubility for tritium. Low pressure breeder gas permeation through the SiC blanket structure is very small (~40 mCi/day). Helium coolant does not significantly contribute to tritium leakage from the plant. See Section 6.7.10.2 for further details. The higher solubility of tritium in the lead coolant requires additional safeguards and permeation barriers. The lead steam generators are a double-walled heat transfer tube design with the interspace filled with sodium. Tritium will continually be extracted from the sodium to maintain a low tritium partial pressure in order to meet the plant tritium loss requirements. Section 6.7.10 discusses the heat transfer media de-tritiation analyses and design approaches.

No analysis was performed for target debris activation; however, with the exception of lead, the constituents of the target are expected to have low activation. Since Pb is already present in the coolant, the same type of radionuclides are produced.

The quantities of the different radioactive first wall, blanket, and shield materials were computed using the DKRICF code for a period of 2 and 30 years of full power operation. (Note: The design life of the first wall is anticipated to be five years and the blanket ten years.) The results of these calculations are discussed in Section 6.8.5.2. Lead presents the largest activation concern and results in a considerable inventory compared to the blanket system. Considerable emphasis was given to bismuth impurity control and removal and the safe storage of ^{210}Po from the lead coolant. All radioactive materials are present either in liquid or solid form. Their release to the

environment under normal operation can be excluded. The Pb radionuclides are classified as elements somewhat volatile in accidents (ESECOM Class III).

Various first wall failure modes with possible consequences are identified and tabulated in Table 6.8.5-1. Within these failure modes, accident analyses were performed for component thermal responses following loss-of-cooling accidents, lead decay heat removal under accident conditions, and first wall behavior due to local dry spots. These analyses provide a guideline for the cavity safety design.

Table 6.8.5-1 Cavity Failure Modes and Consequences

	Failure Mode	Consequences
1.	Failure to drain Pb and to remove the decay heat	Local structure damage, replace FW segment
2.	Loss of coolant in FW with continuing pellet explosions	FW structure damage from blast, closure of interconnected porosity – replace FW segment
3.	Loss of cooling in blanket with continuing pellet explosions	Blanket module temperatures build up, leading to structural failure and/or breeder sintering (causes increased tritium inventory or necessitates blanket replacement)
4.	Loss of flow (pump failure) in FW with pellet explosions	FW overheating and mechanical damage
5.	FW panel local dry spot	Possible FW structure damage, closure of interconnected porosity
6.	FW fatigue due to blast effects	FW panel mechanical failure or damage
7.	Blanket cooling tube rupture (5 MPa design)	Module overpressure, module failure, cascade failures, purge system overpressure, purge system rupture, and tritium release to reactor building
8.	Purge line rupture	Tritium release to reactor building
9.	Pb coolant manifold or pipe rupture	Radioactive leak of Pb to reactor building
10.	He coolant manifold or pipe rupture	Reactor building overpressure, some tritium release

6.8.5.2 Radioactivity in the Cavity – Activation analysis has been performed for the Prometheus IFE first wall, blanket, shield, and cover gas environment as defined in Figure 6.8.5-1. The main constituents of the first wall are the SiC structure and the lead coolant. The blanket uses Li_2O breeder, which has low activation characteristics, with SiC structure and helium coolant. Behind the blanket system, there is a vacuum vessel which is made of 100% ferritic steel and 210 cm of biological shield. (Final

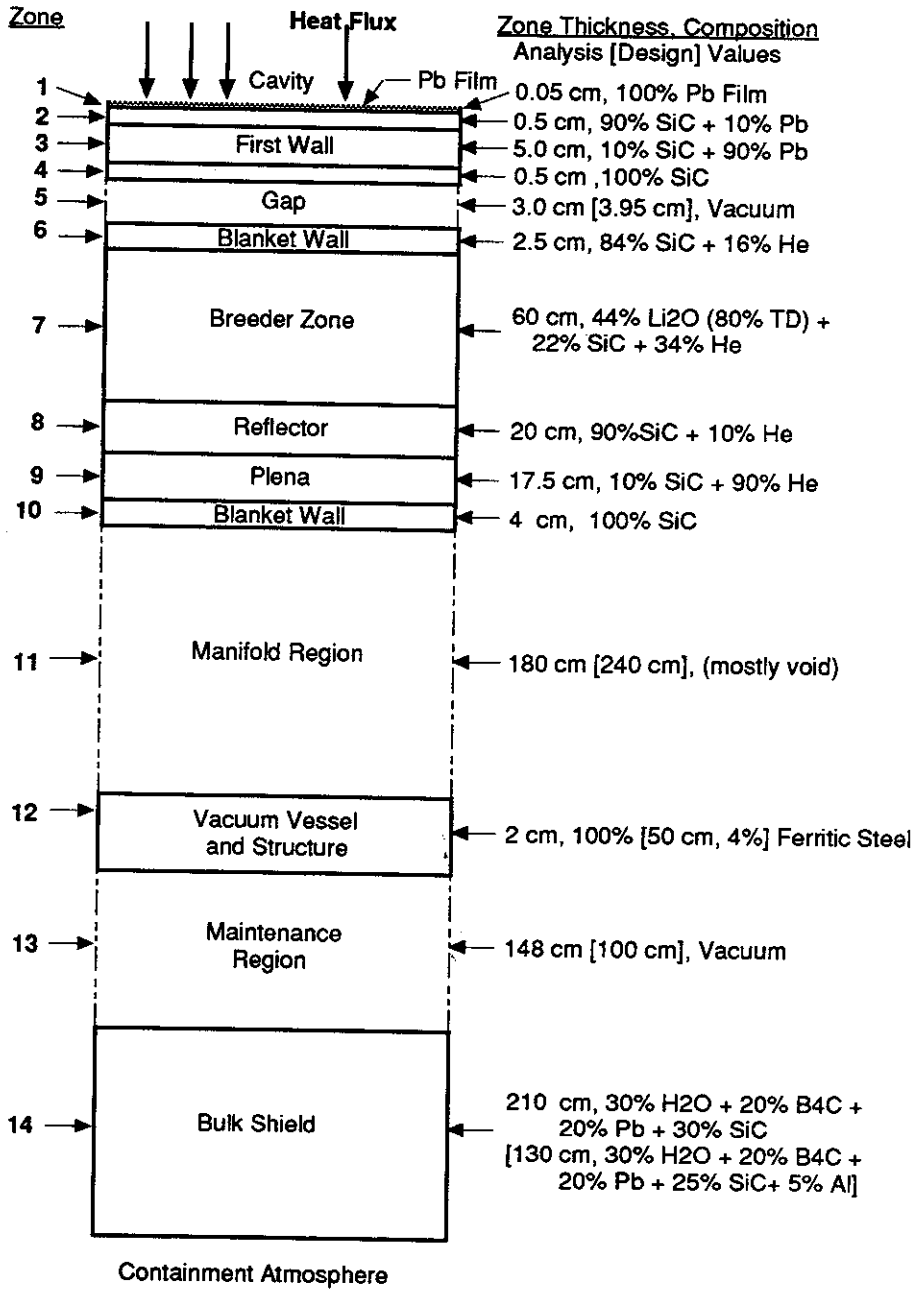

Figure 6.8.5-1 Cavity Cross-Section and Zone Designation

shield thickness is 130 cm.) The shield consists of Al structure, H_2O coolant, and B_4C, Pb, and SiC absorbers. Finally, ordinary air at STP is assumed to surround the cavity. Descriptions of the geometric configuration, dimensions and material volume fraction of the aforementioned components can be found in previous sections.

Calculational Procedure – Figure 6.8.5-2 shows the calculational procedures as well as the codes and libraries used to calculate the radioactivity. A neutron transport calculation was carried out first using ANISN[1] to determine the neutron flux and energy spectrum at various locations in the cavity. During ANISN calculations, a P_3S_8 approximation and the neutron/photon cross section data derived from ENDF/B-V[2] have been employed. The problem has been modeled in spherical geometry with materials and dimensions consistent with a cut through the midplane of the cavity. A point source was used at the center of the 510-cm radius cavity. The SIRIUS-M[3] target neutron spectrum was used to represent the source spectrum. The source neutron strength has been obtained as 9.636×10^{20} n/sec by considering the average neutron energy (12.87 MeV) of the SIRIUS-M source spectrum and the neutron power (1987 MW) of the Prometheus design.

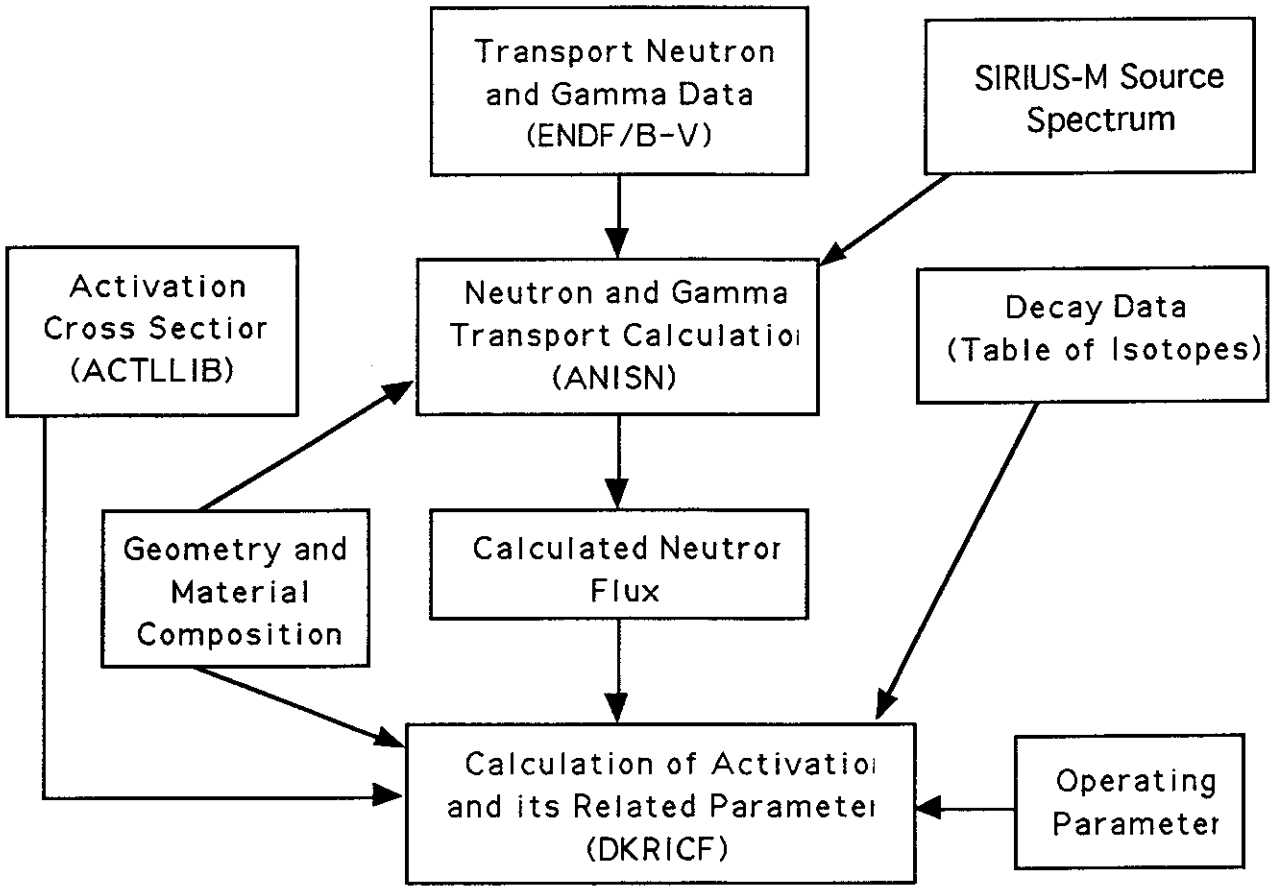

Figure 6.8.5-2 Radioactivity Calculational Procedure

The neutron flux obtained from the neutron transport calculation was used as input to the activation calculation, which used the DKRICF[4] code. For the results reported here, the machine was assumed to operate for 40 years with 75% availability, which corresponds to approximately 30 years of continuous operation at full power. The

blanket and shield were assumed to operate through the entire 30 full-power years (FPY); the first wall system is assumed to be replaced after 2 FPY. Note that a first wall lifetime of 5 FPY and a blanket lifetime of 10 FPY were chosen for the final design point.

The exact time-dependent operation scheme is not considered in this study. It has been reported[5] that even though the employment of continuous operation scheme underestimates the short-term radioactivity production when compared to the actual pulse-shaped operation scheme, the former scheme produces the same amount of long-term (less than one week after shutdown) radioactivity as the latter scheme does. Therefore, the use of continuous operation should not affect the long-term radioactivity calculations in this study.

Results and Discussion

a. Radioactivity - Table 6.8.5-2 summarizes the calculated results as a function of time after shutdown. Table 6.8.5-3 shows the important reaction products and their originating reactions. Figures 6.8.5-3 through 6.8.5-5 are the graphical form of the results presented in Table 6.8.5-2. In the following, specific quantities given for "activation level" refer to specific radioactivity, i.e., radioactivity per unit volume.

In Zone 1, which is 100% Pb film, the activation level at short times after shutdown (0 ~ 1 week) is dominantly governed by the Pb^{203} (2.17d, $Pb^{204}(n,2n)$) and Pb^{209} (3.25h, $Pb^{208}(n,\gamma)$). After that, Tl^{204} (3.78y, $Pb^{204}(n,p)$) takes over the leading role until about 10 years after shutdown. Then, Pb^{205}(1.9×10^{7}y, $Pb^{204}(n,\gamma)$ or $Pb^{206}(n,2n)$) has the responsibility for the very long-term radioactivity level in this zone. The same behavior of the activation level is found in Zone 3, which consists of 10% SiC and 90% Pb, except Al^{28} (2.24 min., $Si^{28}(n,p)$) is one of the major contributors at very short times after shutdown. In Zones 4, 6, 8, 9, and 10 where only SiC is the main material, the activation level in the time span of 0 to ~5 minutes after shutdown is mainly due to Al^{28}.

After most of the Al^{28} decays away, Si^{31} (2.62h, $Si^{30}(n,\gamma)$) becomes the leading contributor between 1 hour ~ 1 day after shutdown. Then, beyond one week after shutdown, Be^{10} (1.6×10^{6}y, $C^{13}(n,\alpha)$) and C^{14} (5.73×10^{3}y, $C^{13}(n,\gamma)$)

Table 6.8.5-2 Zonal Specific Radioactivity (Ci/cm^3) as a Function of Post Shutdown Times After 30 Years Full Operation. Also shown are the Dominating Isotopes and Their Contributions at Each Time. (Except First Wall System Which Is Assumed to Operate for Two Years)

Note: Final Design Determined a Wall Life of 5 Years and a Blanket Life of 10 Years

Post shutdown times	Zone number 1(*)	2(*)	3(*)	4(*)	6	7(+)
0	1.281+1(**) Pb203:59% Pb209:40%	1.093+2 Al28:91%	1.940+1 Al28:37% Pb203:27% Pb209:23%	7.450+1 Al28:93%	5.383+1 Al28:93%	4.791 Al28:77% N16:12%
1 min	1.278+1 Pb203:59% Pb209:40%	7.967+1 Al28:92%	1.676+1 Al28:39% Pb203:31% Pb209:26%	5.429+1 Al28:93%	3.923+1 Al28:93%	2.905 Al28:93%
1 hour	1.165+1 Pb203:64% Pb209:36%	1.305 Pb203:56% Pb209:32%	8.842 Pb203:59% Pb209:41%	1.442-1 Si31:91%	1.014-1 Si31:91%	8.881-3 Si31:93%
1 day	5.560 Pb203: 99%	5.458-1 Pb203:99%	3.884 Pb203:99%	3.001-4 Si31:100%	2.139-4 Si31:99%	3.706-5 Si31:51% C14:49%(@)
1 week	8.383-1 Pb203:96%	8.225-2 Pb203:96%	5.846-1 Pb203:96%	2.846-7 Be10:52% C14:48%	3.105-6 Be10:53% C14:47%	1.829-5 C14:99%(@)
1 month	2.398-2 Hg203:81% Tl204:17%	2.348-3 Hg203:81% Tl204:17%	1.647-2 Hg203:81% Tl204:17%	2.846-7 Be10:52% C14:48%	3.105-6 Be10:53% C14:47%	1.829-5 C14:99%(@)
1 year	3.541-3 Tl204:96%	3.473-4 Tl204:96%	2.437-3 Tl204:96%	2.846-7 Be10:52% C14:48%	3.105-6 Be10:52% C14:48%	1.829-5 C14:99%(@)
5 years	1.642-3 Tl204:99%	1.614-4 Tl204:99%	1.132-3 Tl204:99%	2.846-7 Be10:52% C14:48%	3.105-6 Be10:53% C14:47%	1.829-5 C14:99%(@)
10 years	6.632-4 Tl204:98%	6.560-5 Tl204:97%	4.567-4 Tl204:98%	2.846-7 Be10:52% C14:48%	3.105-6 Be10:53% C14:47%	1.829-5 C14:99%(@)
100 years	1.320-5 Pb205:100%	1.653-6 Pb205:78% Be10:13% C14:9%	9.224-6 Pb205:99%	2.827-7 Be10:52% C14:42%	3.081-6 Be10:53% C14:47%	1.807-5 C14:99%(@)
1,000 years	1.320-5 Pb205:100%	1.640-6 Pb205:79% Be10:13% C14:8%	9.224-6 Pb205:99%	2.687-7 Be10:55% C14:45%	2.940-6 Be10:56% C14:44%	1.620-5 C14:99%(@)
10,000 years	1.320-5 Pb205:100%	1.543-6 Pb205:84% Be10:13%	9.224-6 Pb205:99%	1.878-7 Be10:78% C14:22%	2.070-6 Be10:79% C14:21%	5.531-6 C14:98%(@)

(*) Two years of operation assumed for first wall system

(**) Read as 1.218 x 10^1

(+) Excluding tritium activation

(@) ^{14}C values in Zone 7 were obtained using the DKRICF cross-section library. Due to an error found in this library, the actual values are expected to be much lower (see text).

Table 6.8.5-2 Zonal Specific Radioactivity (Ci/cm^3) as a Function of Post Shutdown Times After 30 Years Full Operation. (Continued)

Post shutdown times	Zone number 8	9	10	12	14	15
0	9.187-1 Al28:92%	3.376-2 Al28:90%	2.479-1 Al28:90%	8.308-1 W187:44% Cr51:8% Fe55:27%	1.186-3 Al28:62% T:15% Li8:8%	8.270-17 Cl38:27% S37:25% S35:24% C14:17%
1 min	6.766-1 Al28:92%	2.504-2 Al28:89%	1.885-1 Al28:89%	8.283-1 W187:44% Cr51:8% Fe55:27%	8.323-4 Al28:65% T:21%	7.962-17 Cl38:27% S37:23% S35:25% C14:17%
1 hour	1.244-2 Si31:99%	9.344-4 Si31:99%	6.852-3 Si31:99%	7.840-1 W187:45% Cr51:8% Fe55:29%	2.453-4 T:72% Pb209:17%	4.664-17 S35:42% C14:29% Cl38:16%
1 day	2.821-5 Si31:99%	2.131-6 Si31:99%	1.562-5 Si31:99%	5.628-1 W187:32% Cr51:11% Fe55:40%	1.938-4 T:91%	3.812-17 S35:52% C14:36%
1 week	1.321-7 C14:76% Be10:24%	8.933-9 C14:87% Be10:13%	6.527-8 C14:87% Be10:13%	3.354-1 Fe55:65% Cr51:16%	1.791-4 T:99%	3.697-17 S35:51% C14:37%
1 month	1.321-7 C14:76% Be10:24%	8.933-9 C14:87% Be10:13%	6.527-8 C14:87% Be10:13%	3.003-1 Fe55:77% Cr51:10% Mn54:9%	1.760-4 T:99%	3.316-17 S35:47% C14:41%
1 year	1.319-7 C14:77% Be10:23%	8.933-9 C14:87% Be10:13%	6.527-8 C14:87% Be10:13%	1.883-1 Fe55:92%	1.670-4 T:99%	1.741-17 C14:79% Ar39:15%
5 years	1.319-7 C14:77% Be10:23%	8.926-9 C14:88% Be10:12%	6.502-8 C14:87% Be10:13%	6.277-2 Fe55:99%	1.333-4 T:99%	1.627-17 C14:84% Ar39:15%
10 years	1.319-7 C14:77% Be10:23%	8.926-9 C14:87% Be10:13%	6.502-8 C14:87% Be10:13%	1.729-2 Fe55:99%	1.005-4 T:99%	1.622-17 C14:85% Ar39:15%
100 years	1.308-7 C14:76% Be10:24%	8.840-9 C14:87% Be10:13%	6.450-8 C14:87% Be10:13%	3.243-4 Nb93m:70% Mo93:24%	6.343-7 T:99%	1.557-17 C14:87% Ar39:13%
1,000 years	1.205-7 C14:74% Be10:26%	8.046-9 C14:86% Be10:14%	5.882-8 C14:86% Be10:14%	2.745-4 Nb93m:70% Mo93:23%	3.711-9 C14:60% Be10:23% Pb205:17%	1.238-17 C14:99%
10,000 years	6.118-8 Be10:51% C14:49%	3.443-9 C14:68% Be10:32%	2.518-8 C14:68% Be10:32%	5.809-5 Nb93:55% Mo93:23% Nb94:19%	2.227-9 Be10:39% C14:33% Pb205:28%	4.103-18 C14:100%

Table 6.8.5-3 Reaction Products Resulting from the Neutron Irradiation of Reactor Materials

Product	Half-Life	Originating Reaction
T	12.3 y	$B^{10}(n,2\alpha)$
Be^{10}	1.6×10^{6} y	$C^{13}(n,\alpha)$
C^{14}	5.73×10^{3} y	$C^{13}(n,\gamma)$ $N^{14}(n,p)$, $O^{17}(n,\alpha)$
N^{16}	7.13 sec	$O^{16}(n,p)$
Al^{28}	2.24 min	$Al^{27}(n,\gamma)$ $Si^{28}(n,p)$, $Si^{29}(n,np/d)$
Si^{31}	2.62 h	$Si^{30}(n,\gamma)$
S^{35}	87.5 d	$Ar^{38}(n,\alpha)$
S^{37}	5.1 min	$Ar^{40}(n,\alpha)$
Cl^{38}	55.6 m	$Ar^{38}(n,p)$
Ar^{39}	269 y	$Ar^{38}(n,\gamma)$, $Ar^{40}(n,2n)$
Mn^{54}	312.2 d	$Fe^{54}(n,p)$, $Fe^{56}(n,t)$
Fe^{55}	2.73 y	$Fe^{54}(n,\gamma)$, $Fe^{56}(n,2n)$
Nb^{93m}	13.6 y	$Nb^{93}(n,\gamma)^{*}$ $Mo^{92}(n,\gamma)Mo^{93}\rightarrow Nb^{93m}$ $Mo^{94}(n,2n)Mo^{93}\rightarrow Nb^{93m}$ $Mo^{94}(n,2n)^{*}Mo^{93m}\rightarrow Mo^{93}\rightarrow Nb^{93m}$ $Mo^{95}(n,3n)Mo^{93}\rightarrow Nb^{93m}$
Nb^{94}	2.0×10^{4} y	$Nb^{93}(n,\gamma)$ $Nb^{93}(n,\gamma)^{*}Nb^{94m}\rightarrow Nb^{94}$ $Mo^{94}(n,p)$, $Mo^{95}(n,np/d)$, $Mo^{96}(n,t)$
Mo^{93}	3.5×10^{3} y	$Mo^{92}(n,\gamma)$, $Mo^{94}(n,2n)$ $Mo^{94}(n,2n)Mo^{93m}\rightarrow Mo^{93}$
W^{187}	23.9 h	$W^{186}(n,\gamma)$
Hg^{203}	46.6 d	$Pb^{206}(n,\alpha)$, $Pb^{207}(n,n\alpha)$
Tl^{204}	3.78 y	$Pb^{204}(n,p)$, $Pb^{206}(n,t)$
Pb^{203}	2.17 d	$Pb^{204}(n,2n)$
Pb^{205}	1.9×10^{7} y	$Pb^{204}(n,\gamma)$, $Pb^{206}(n,2n)$
Pb^{209}	3.25 h	$Pb^{208}(n,\gamma)$, $Bi^{209}(n,p)$

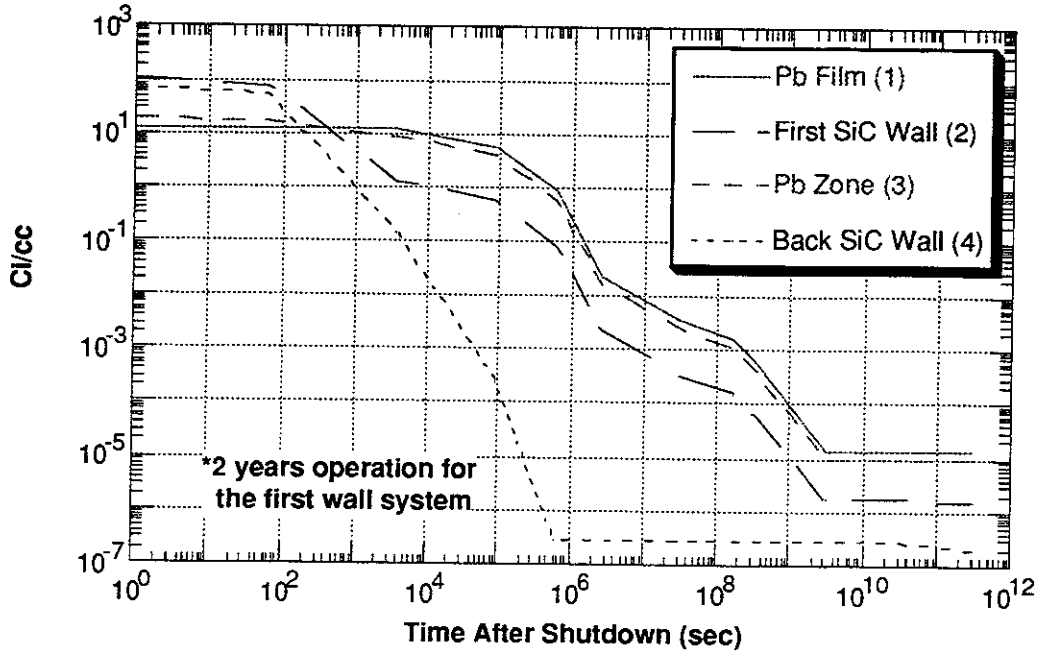

Figure 6.8.5-3 Specific Radioactivity in the First Wall System

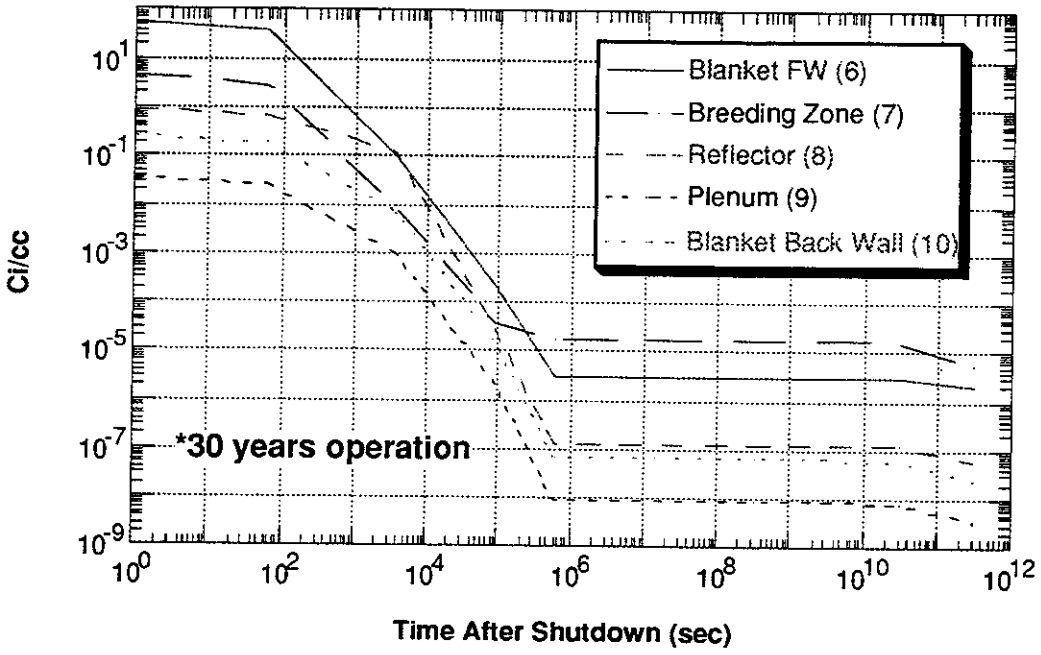

Figure 6.8.5-4 Specific Radioactivity in the Blanket and Reflector

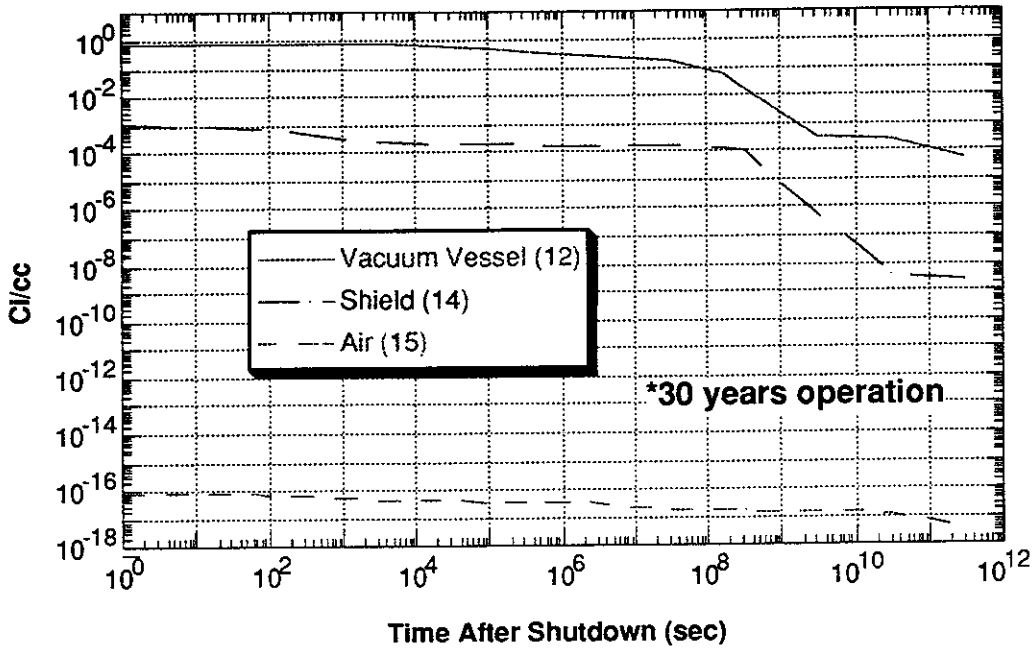

Figure 6.8.5-5 Specific Radioactivity in the Vacuum Vessel, Shield, and Surrounding Air

are responsible for the activation levels in these zones. Zone 2 (90% SiC and 10% Pb) has characteristics between the pure lead and pure SiC zones. Refer to Table 6.8.5-2 for the specific information on this zone.

Activation levels in Zone 7, which is the breeding zone, come mostly from the SiC structure and are governed primary by Al^{28} for the short-term and C^{14} for the long- and very long-term after shutdown radioactivity. Tritium activation was not included in this zone since most of tritium will be extracted and processed separately for future use. Note that C^{14} can be produced by two reaction channels in this zone — $C^{13}(n,\gamma)$ and $O^{17}(n,\alpha)$.

In the process of performing these calculations, it was discovered that the cross section library of DKRICF contains data for the $^{17}O(n,x)$ cross section which is highly suspect. The calculation was performed using the more plausible data from THIDA-2,[6] and the resulting zone-averaged ^{14}C radioactivity level in the breeding zone (Zone 7) is shown in Table 6.8.5-4. The long-term radioactivity is reduced by two orders of magnitude as compared with Table 6.8.5-2, easily meeting Class C waste disposal limits.

The activation characteristic of the vacuum vessel zone, which is made of ferritic steel, is more complex than the other zones because there are larger

Table 6.8.5-4 Zone-Averaged ^{14}C Radioactivity Level in Breeding Zone (Zone 7) After 30 Years, Using the THIDA-2 Cross Section Library

Time	Radioactivity from SiC (Ci/cc)	Radioactivity from Li_2O (Ci/cc)	Total
0	5.90-9 (a)	1.04-7	1.09-7
1 m	"	"	"
1 h	"	"	"
1 d	"	"	"
1 w	"	"	"
1 mo	"	"	"
1 yr	5.00-9	1.04-7	1.09-7
5 yr	"	"	"
10 yr	"	"	"
100 yr	4.80-9	1.03-7	1.08-7
1,000 yr	4.36-9	9.23-8	9.67-8
10,000 yr	1.48-9	3.11-8	3.26-8

(a) Read as 5.90×10^{-9}

numbers of isotopes involved. Briefly, W^{187} (23.9h, $W^{186}(n,\gamma)$), Fe^{55} (2.73y, $Fe^{56}(n,2n)$), and Nb^{93m} (13.6y, $Nb^{93}(n,n')^*$) are the important contributors for the short-, long-, and very long-term after shutdown radioactivity, respectively.

In the shield zone (Zone 14), which is composed of $B_4C+H_2O+Pb+SiC$, tritium is the most dominating radionuclide during 1 hour to 100 years after shutdown. Tritium is produced via $B^{10}(n,2a)$ reaction in this zone. The air activation (Zone 15), which is assumed to surround the reactor cavity, is also estimated. At shutdown, the activation of air is lower than that of the shield by 14 orders of magnitude. However, the air activation does not decay as fast as the other zones do, since C^{14} ($T_{1/2}$ = 5730 years) is the major radionuclide. During 10,000 years after shutdown, the air activation decays to only 5% of the activation level at shutdown.

Figure 6.8.5-6 compares the integrated radioactivity (in Curies) in the first wall, blanket, vacuum vessel, and shield regions. The following observations are made on the results in Figure 6.8.5-6:

(1) The radioactivity inventory of the total cavity at shutdown is about 2.5×10^9 Curies, which can be translated into ~0.9 Ci/W of thermal power. This value is comparable to that in other IFE design studies such as HIBALL[7] or in typical MCF designs such as ITER.[8]

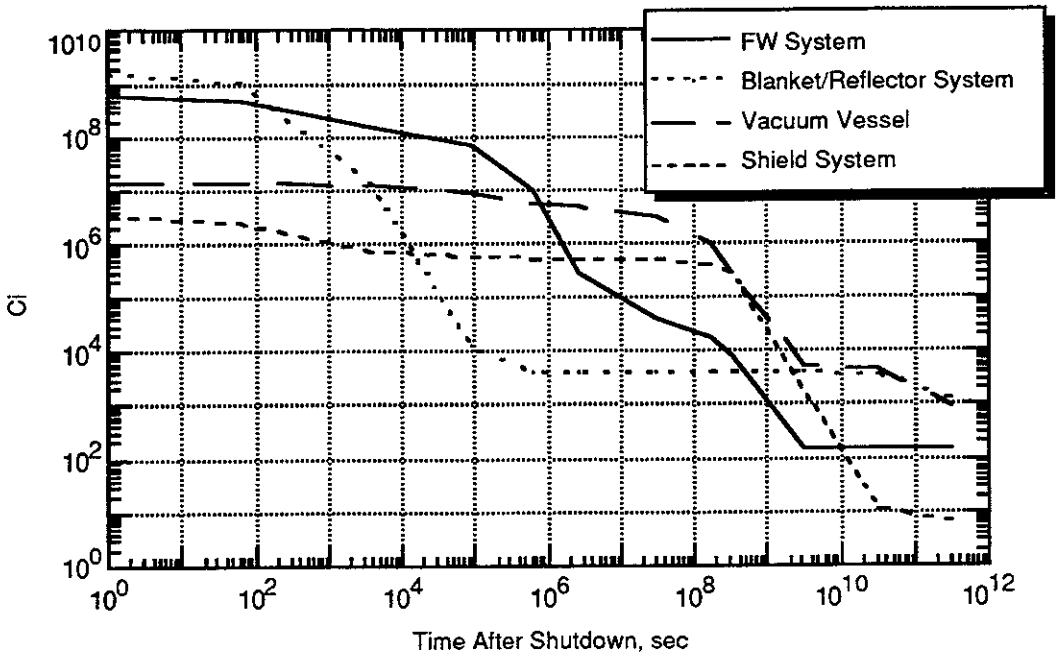

Figure 6.8.5-6. Integrated Radioactivity in Each Component as a Function of Time After Shutdown

(2) The blanket/reflector system has the highest radioactive inventory for both very short-term (less than a few minutes) and very long-term (greater than 100 years) after shutdown. The short term activity is mainly due to Al^{28} and the long-term is due to C^{14} and Be^{10}.

(3) The activation level in the first wall protection system does not decay as quickly as the blanket system does since it contains the Pb. In the first wall system, the long-term activities are mainly due to the reaction products from Pb.

(4) Even though it has the smallest volume of all systems, the vacuum vessel has the largest activation inventory because of the use of ferritic steel which results in much higher long-term radioactivity than that from the SiC/SiC composite used as the structural material in the other zones.

Also, the radioactivity inventory comparison study between our shield and a conventional concrete shield, which is made of 87% concrete + 8% ferritic steel + 5% H_2O, has been performed and the results are shown in Figure 6.8.5-7. As shown, the activation level of the Prometheus shield is always less than that of the concrete shield by one to three orders of magnitude. The use of ferritic steel could result in higher activation in the conventional concrete shield. The

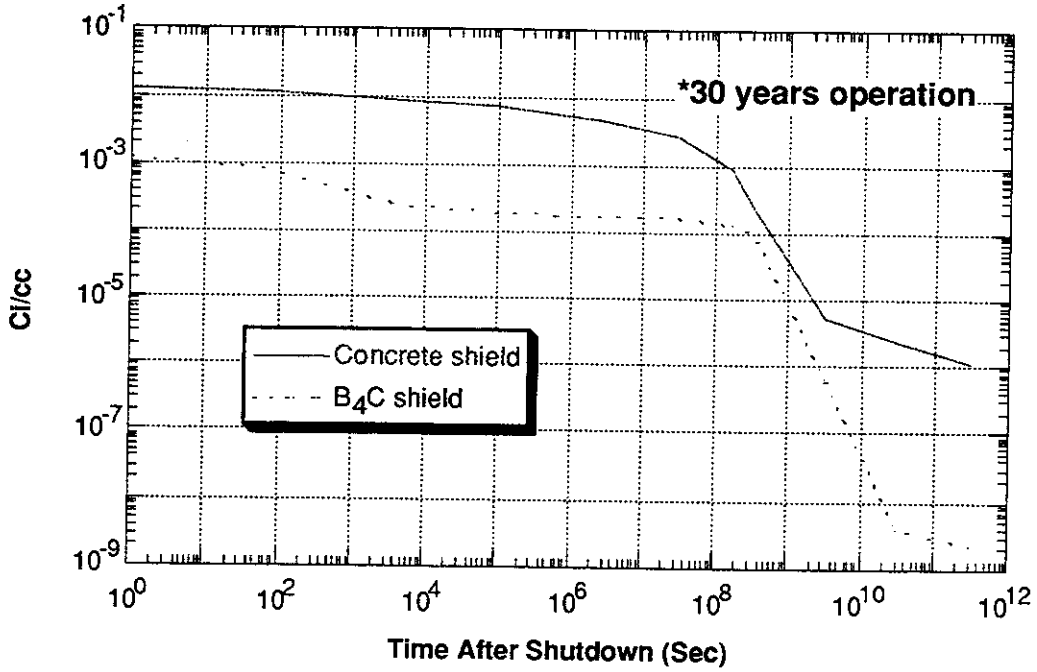

Figure 6.8.5-7. Comparison of Activation Levels Between Prometheus and Conventional Concrete Shield

use of B_4C gives lower activation in our shield design, since boron is a very strong neutron absorber so that the average population of low-energy neutrons in B_4C shield will be less than that in a concrete shield. The neutron and the photon fluxes during operation right behind the two different shields are displayed in Figures 6.8.5-8 and 6.8.5-9, respectively. It is apparent that the B_4C shield blocks or absorbs the large number of lower energy neutrons. The photon flux is also lower by about six orders of magnitude in the B_4C shield. Accordingly, the dose rate behind the B_4C shield will be much less than that behind the conventional concrete shield during reactor operation.

It has to be noted at this point that, by adopting the spherical geometry modeling, the results reported in this paper are conservative. In other words, if we consider the actual cylindrical modeling, the average activation level will be less than the results given here. This is because we have a point neutron source at the center of the cavity so that the neutron flux at position B (Figure 6.8.5-10) will be less than that at position A by roughly a factor of R_A^2/R_B^2. The average flux incident on the first wall can be obtained as:

[Text Continues on Page 6.8.5-15]

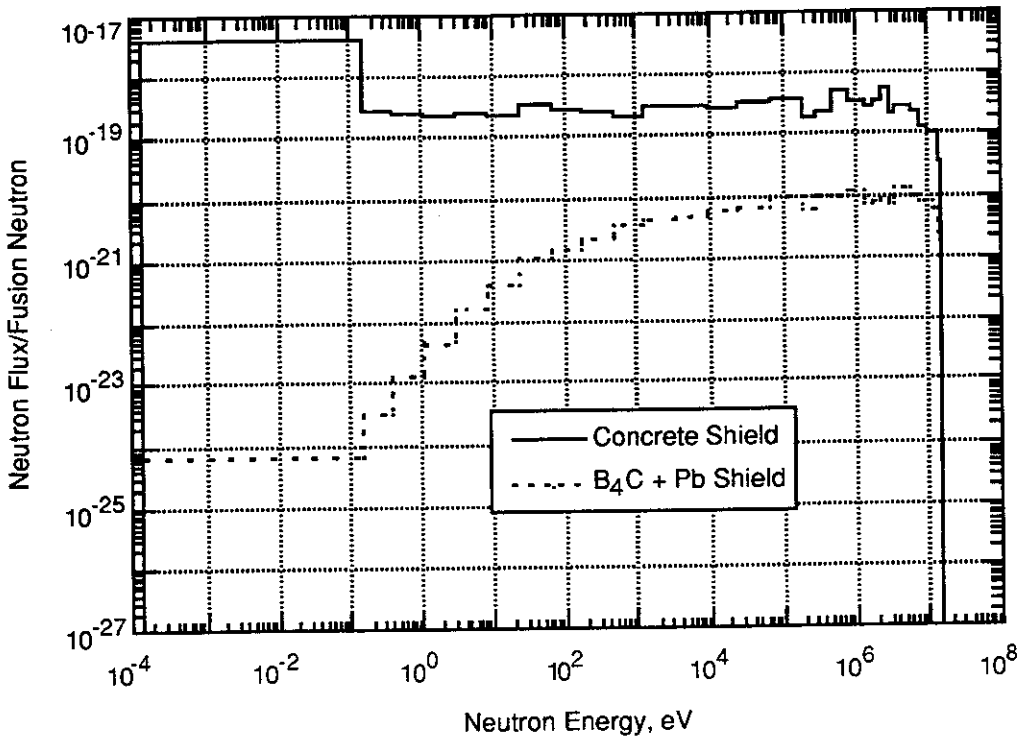

Figure 6.8.5-8. Neutron Flux Comparison Between Prometheus and Conventional Concrete Shield

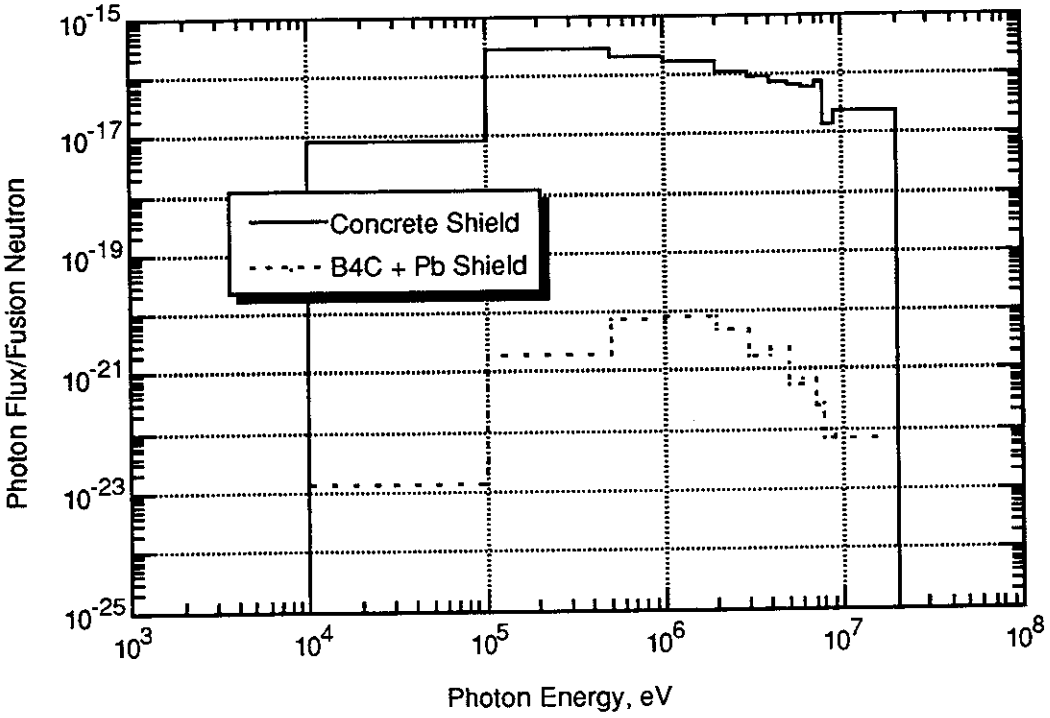

Figure 6.8.5-9. Photon Flux Comparison Between Prometheus and Conventional Concrete Shield

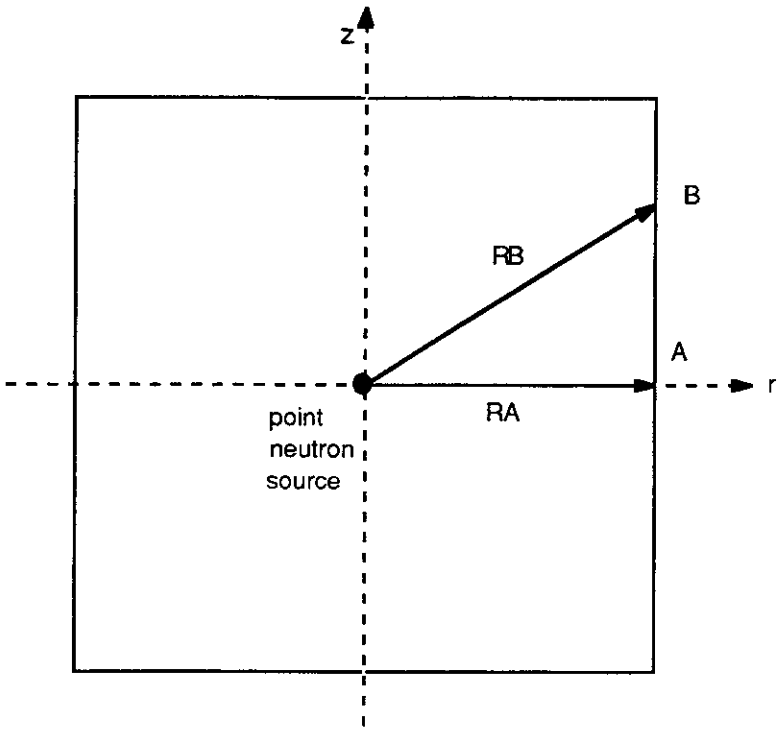

Figure 6.8.5-10. Cylindrical Modeling of the Cavity

[Text Continues from Page 6.8.5-13]

$$\phi_B = \frac{\phi_A}{\left[1+\left(\frac{z}{R}\right)^2\right]}$$

$$<\phi> = \phi_A \frac{\int_0^H \frac{dz}{1+(z/R)^2}}{\int_0^H dz}$$

$$= \phi_A \frac{R}{H}\tan^{-1}\left(\frac{H}{R}\right) \qquad (6.8.5.2\text{-}1)$$

In the above equation, ϕ_A is the flux at z=0 and H is the half-height of the cylinder. Therefore, if one is to be more accurate, one has to replace the flux term with the Eq. (6.8.5.2-1) in all the balance equations. As an example, let us consider the most common and simplest reaction/decay chain: A(n,x)B $\rightarrow$ C. Now we have a following set of equations.

$$\frac{dN_A}{dt} = -\sigma\phi N_A$$

$$\frac{dN_B}{dt} = \sigma\phi N_A - \lambda N_B$$
$$\frac{dN_C}{dt} = \lambda N_B$$

Then, without the average flux consideration, we have:

$$N_B(t) = \frac{\sigma\phi_A N_{A0}}{1-\sigma\phi_A}\left(e^{-\sigma\phi_A t} - e^{-\lambda t}\right).$$

Now, with the average flux, we have:

$$\langle N_B(t)\rangle = \frac{\sigma\langle\phi\rangle N_{A0}}{1-\sigma\langle\phi\rangle}\left(e^{-\sigma\langle\phi\rangle t} - e^{-\lambda t}\right).$$

Therefore, we get:

$$\frac{\langle N_B(t)\rangle}{N_B(t)} = \frac{\langle\phi\rangle}{\phi_A}\frac{\lambda-\sigma\phi_A}{\lambda-\sigma\langle\phi\rangle}\frac{e^{-\sigma<\phi>t} - e^{-\lambda t}}{e^{-\sigma\phi_A t} - e^{-\lambda t}} \qquad (6.8.5.2\text{-}2)$$

Two extreme cases are interesting: (1) $\lambda >> \sigma\phi$ or $\sigma<\phi>$ and (2) $\lambda << \sigma\phi$ or $\sigma<\phi>$. In Case 1, Eq. (6.8.5.2-2) becomes

$$\frac{<N_B(t)>}{N_B(t)} \sim \frac{<\phi>}{\phi_A} e^{-\sigma\phi_A\left(\frac{<\sigma>}{\phi_A}+1\right)t}$$
$$= \frac{R}{H}\tan^{-1}\left(\frac{H}{R}\right) e^{-\sigma\phi_A\left[\frac{H}{R}\tan^{-1}\left(\frac{R}{H}\right)+1\right]t} \qquad (6.8.5.2\text{-}3)$$

For Case 2, Eq. (6.8.5.2-2) becomes

$$\frac{<N_B(t)>}{N_B(t)} \sim \frac{<\phi>}{\phi_A}\frac{\sigma\phi_A}{\sigma<\phi>}\frac{e^{-\lambda t}}{e^{-\lambda t}} = 1,$$

which means that accounting for the difference in the average flux is not necessary for the very long half-life radioactive products. With the typical values of $\phi_A \sim 10^{15}$ n/cm^{2}sec, $\sigma \sim 0.1$ barn, t ~ 1 year operation, and R=H=5m, $\frac{<N_B>}{N_B} \sim 0.78$ for Case 1. Therefore, the average activity in the Prometheus first wall protection system will be about 20% less than the values reported in Table 6.8.5-2, especially for the products whose half-lives satisfy the condition of $T_{1/2} << \sigma\phi_A$ or $\sigma<\phi>$.

b. Biological Hazard Potential (BHP) – In addition to the magnitude of radioactivity, the BHP values in each zone have been computed and the results are shown in Figures 6.8.5-11 through 6.8.5-13 as a function of time

after shutdown. The BHP is a measure of the "Biological Hazard" of the radioactivity in various materials.

Figure 6.8.5-11 shows the BHP values in the first wall system. It shows that the lead containing zones (Zone #1 and #3) have the highest BHP values among the other zones all the time. The products such as Pb^{209} (3.25h, $Pb^{208}(n,\gamma)$) for short times after shutdown and Pb^{205}($1.9x10^7$y, $Pb^{204}(n,\gamma)$ or $Pb^{206}(n,2n)$) for long times after shutdown are responsible for the high BHP values in the Pb zone. In SiC zones (Zone #2 and #4), Al^{28} (2.24 min, $Si^{28}(n,p)$) is dominating

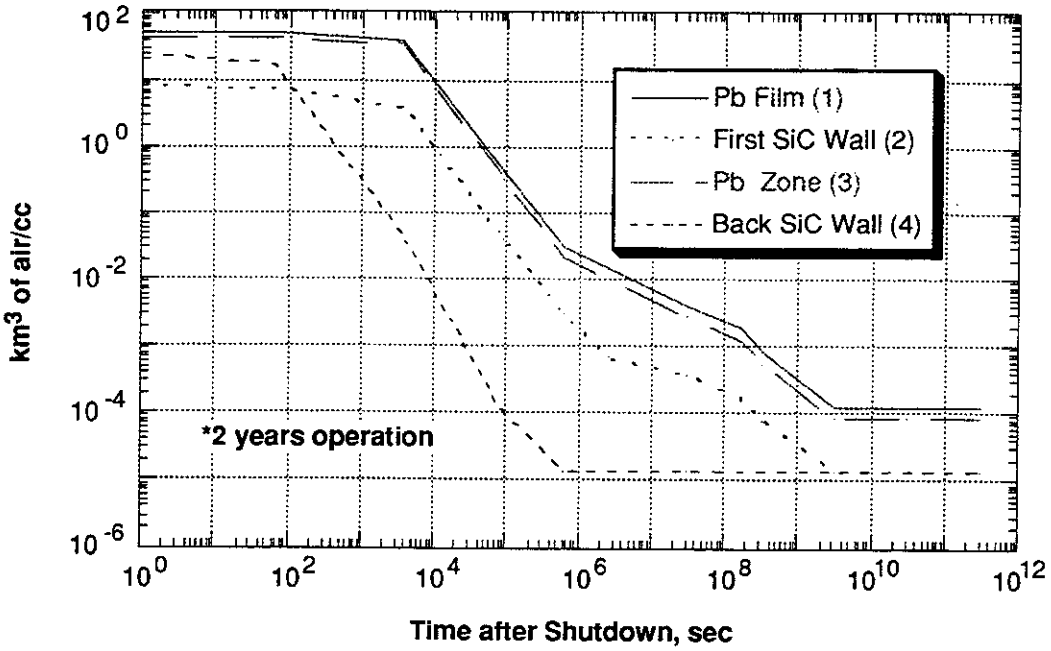

Figure 6.8.5-11. Specific BHP in the First Wall System

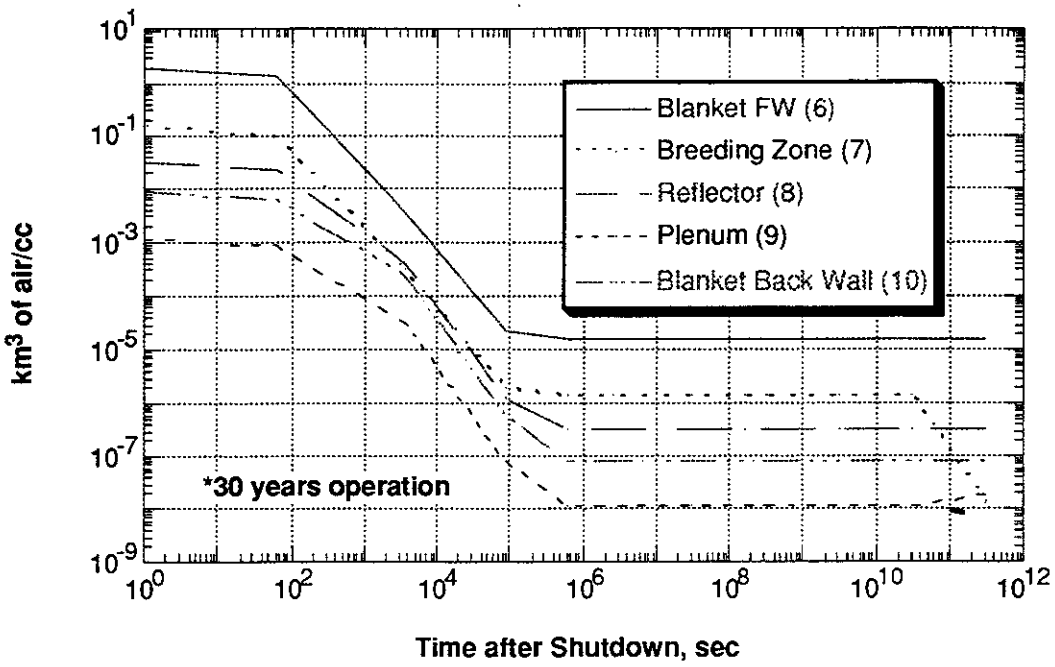

Figure 6.8.5-12. Specific BHP in the Blanket and Reflector

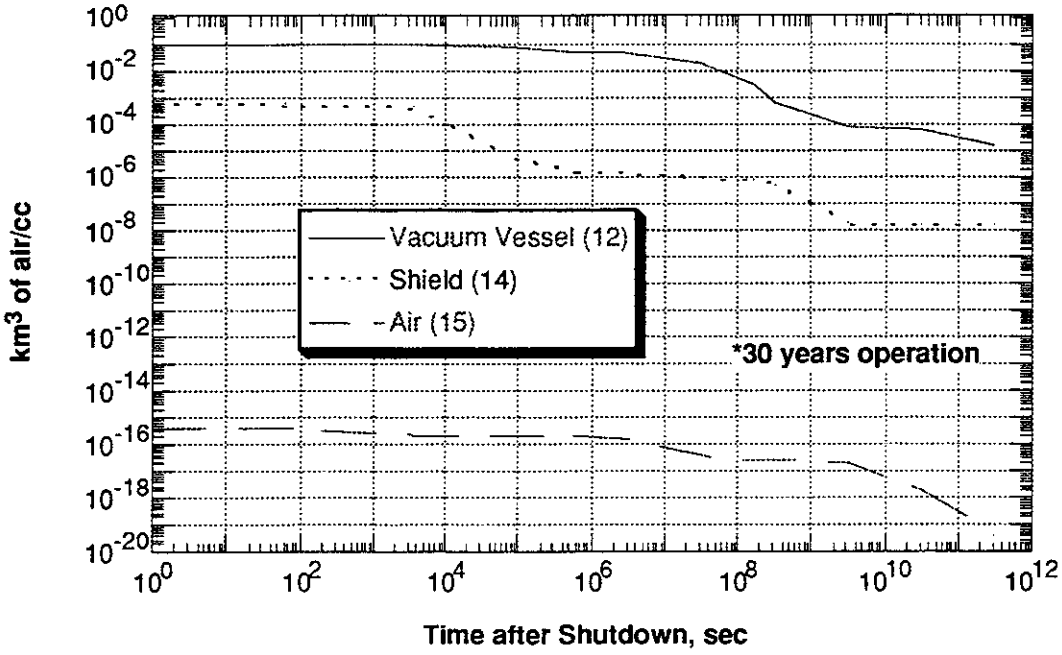

Figure 6.8.5-13. Specific BHP in the Vacuum Vessel, Shield, and Surrounding Air

the BHP values for very short times after shutdown. After Al^{28} decays away, Be^{10} ($1.6x10^6$y, $C^{13}(n,\alpha)$) and C^{14} ($5.73x10^3$y, $C^{13}(n,\gamma)$) take over the leading role in the SiC zone. But, in general, the SiC zone has about 1~3 orders of magnitude lower BHP than the lead zone.

Figure 6.8.5-12 shows the specific BHP values in the blanket and reflector system. Since the SiC is the main material here, every zone in this system shows the same general trend. Furthermore, the deeper the zone is, the lower the BHP values are, because the average neutron flux is less in deeper zones. Figure 6.8.5-13 shows the specific BHP values in the vacuum vessel, shield, and the air around the cavity. Their general trend is found to be very similar to that of the magnitude of radioactivity discussed before for these zones. However, it has to be noted that Mn^{54} ($T_{1/2}$=312.2 day, $Fe^{54}(n,p)$) is the main contributor for the BHP in the vacuum vessel zone in the time span from shutdown to a few years after shutdown. Other important nuclides include W^{187} (23.9h, $W^{186}(n,\gamma)$), Fe^{55} (2.73y, $Fe^{56}(n,2n)$), and Nb^{93m} (13.6y, $Nb^{93}(n,n')^*$) in the vacuum vessel zone. The BHP in the shield zone is governed by Al^{28}, T, Be^{10}, and Pb^{205} for the very short-, long-, and very long-after shutdown times, respectively.

A particular concern in using lead in a high neutron field is the production of Po^{210}. Po^{210} is an α-emitter and volatile. Bismuth is a common impurity in natural lead. The neutron capture reaction with Bi^{209}, which is the only stable nuclide in bismuth, can result in the production of Po^{210}: $Bi^{209}(n,\gamma)Bi^{210} \rightarrow Po^{210}$. Other reaction/decay chains which can produce the Po^{210} are:

$$Pb^{208}(n,\gamma)Pb^{209} \rightarrow Bi^{209}(n,\gamma)Bi^{210} \rightarrow Po^{210} \quad : \text{chain \#1}$$
$$Pb^{208}(n,\gamma)Pb^{209}(n,\gamma)Pb^{210} \rightarrow Bi^{210} \rightarrow Po^{210} \quad : \text{chain \#2}$$

In general, there has been a deficiency in the literature of exact estimations of the Po^{210} production rate from the above two reaction/decay chains, even though it has important safety implications. In this work, a detailed estimation of the Po^{210} production from the first wall system in the Prometheus design has been made based on the available cross section and decay data. The necessary cross section data has been extracted from the activation cross section library in DKRICF and the decay data in the Table of Radioactive Isotopes[9] have been used. All three reaction/decay chains are considered. The bismuth impurity in the natural lead has been taken as 40 wppm throughout the calculation.

First, the results of radioactivity calculations for Po^{210} in the lead film zone using DKRICF are presented in Tables 6.8.5-5 and 6.8.5-6 as a function of time after shutdown. Table 6.8.5-5 shows the radioactivity and Table 6.8.5-6 shows the BHP.

Table 6.8.5-5 Radioactivity (Ci/cm^3) of Po^{210} With Other Dominating Nuclides in the Pb Film

	Total	Most Dominant	Second Dominant	Third	Fourth	Po^{210}
At Shutdown	6.897	Pb^{203}: 3.977	Pb^{209}: 2.853	Hg^{205}: 4.362-2(a)	Hg^{203}: 1.611-2	1.054-4
1 min	6.879	Pb^{203}: 3.976	Pb^{209}: 2.309	Hg^{205}: 3.844-2	Hg^{203}: 1.641-2	1.054-4
1 hour	6.255	Pb^{203}: 3.924	Pb^{209}: 2.309	Hg^{203}: 1.610-2	Tl^{204}: 7.576-3	1.054-4
1 day	2.930	Pb^{203}: 2.889	Pb^{209}: 1.789-2	Hg^{203}: 1.588-2	Tl^{204}: 7.570-3	1.053-4
1 week	4.467-1	Pb^{203}: 4.243-1	Hg^{203}: 1.452-2	Tl^{204}: 7.546-3	Pb^{205}: 1.390-4	1.040-4
1 month	1.829-2	Hg^{203}: 1.032-2	Tl^{204}: 7.460-3	Pb^{203}: 2.719-4	Pb^{205}: 1.390-4	9.400-5
1 year	6.538-3	Tl^{204}: 6.304-3	Pb^{205}: 1.389-4	Hg^{203}: 1.099-4	—	1.756-5

(a) Read as 4.362×10^{-2}

Table 6.8.5-6 BHP (km^3 of Air/cm^3) of Po^{210} With Other Dominating Nuclides in the Pb Film

	Total	Most Dominant	Second Dominant	Third	Fourth	Po^{210}
At Shutdown	2.863+1	Pb^{209}: 2.85+1(a)	Pb^{203}: 6.634-2	—	—	1.756-2
1 min	2.853+1	Pb^{209}: 2.841+1	Pb^{203}: 6.628-2	—	—	1.756-2
1 hour	2.319+1	Pb^{209}: 2.310+1	Pb^{203}: 6.542-2	—	—	1.756-2
1 day	2.627-1	Pb^{209}: 1.789-1	Pb^{203}: 4.815-2	—	—	1.756-2
1 week	4.166-2	—	—	—	—	1.734-2
1 month	3.053-2	—	—	—	—	1.566-2
1 year	1.136-2	Tl^{204}: 7.007-3		—	—	2.922-3

(a) Read as 2.853×10^{1}

The results shown in these tables do not include the effect of build-up of Po^{210} from neutron interactions with natural lead (Chains #1 and #2). Even though the activity level of Po^{210} is small compared to the other dominant radionuclides, it has rather high BHP values because of the much lower maximum permissible concentration, especially during the period of time from one week to a few months after shutdown.

Figure 6.8.5-14 shows the Po^{210} build-up from each of the three reaction/decay chains described above as a function of irradiation time. It is apparent that the production of Po^{210} from the bismuth impurity is more important among the three chains up to about one year irradiation. After that, Chain #1 is mainly responsible for the Po^{210} production. Chain #2 is the least source of the Po^{210} until the irradiation time reaches about 10 years. Then the Po^{210} production from this chain exceeds that from the bismuth impurity. While the Po^{210} production from the Bismuth impurity in lead can be controlled since the Bismuth impurity in lead can be reduced with the extra purifying process, we do not have much control over the production of Po^{210} from Chains #1 and #2. However, replacing lead every year or so can reduce the production of Po^{210} from the lead reaction/decay chain. The isotopic tailoring method, which reduces the Pb^{208} content from the natural lead, can be one solution, but the extra cost is a major concern.

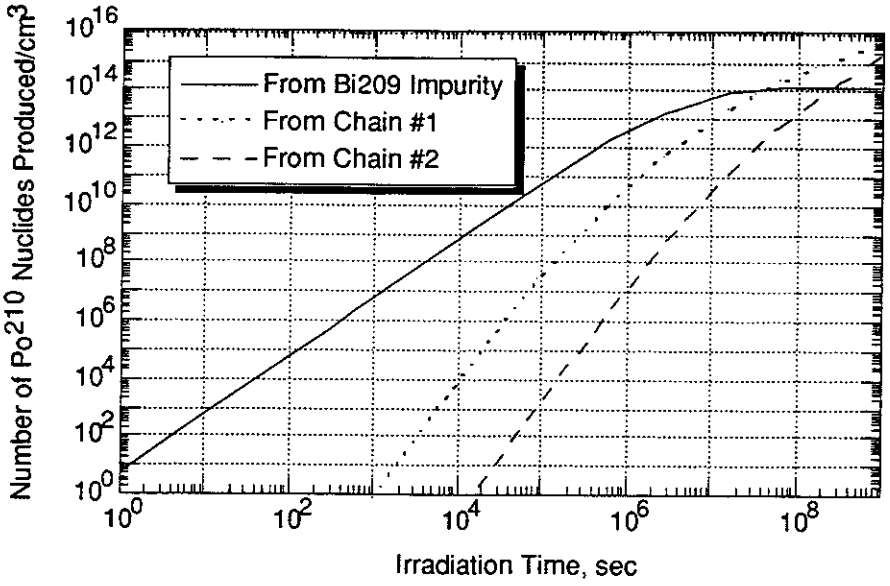

Figure 6.8.5-14 Po^{210} Buildup in the Prometheus First Wall System

References for 6.8.5.2

1. W. W. Engle, Jr., "User's Manual for ANISN, A One-Dimensional Discrete Ordinates Transport Code with Anisotropic Scattering," K-1693, Oak Ridge Gaseous Diffusion Plant (1967).

2. R. R. Kinsey, Compiler, "Evaluated Neutron Data File, ENDF/B-V," ENDF Summary Documentation, ENDF-201, 3rd Edition, BNL (1979).

3. B. Badger, S. I. Abdel-Khalik, H. M. Attaya, et al., "SIRIUS-M: A Symmetric Illumination, Inertially Confined Direct Drive Materials Test Facility," UWFDM-711 (1986).

4. D. L. Handerson and Osman Yasar, "DKRICF: A Radioactivity and Dose Rate Calculation Code Package," UWFDM-714 (1986).

5. H. Y. Khater and M. E. Sawan, "Dose Rate Calculations for a Light Ion Beam Fusion Laboratory Microfusion Facility," UWFDM-809 (1989).

6. Y. Seki, et al., "THIDA-2: An Advanced Code System for Calculation of Transmutation, Activation, Decay Heat and Dose Rate," RSIC Computer Code Collection, CCC-410 (April 1987).

7. B. Badger, F. Arendt, K. Becker, et al., "HIBALL: A Conceptual Heavy Ion Beam Driven Fusion Reactor Study," UWFDM-450 (1981).

8. H. Attaya, Y. Gohar, and D. Smith, "US-ITER Activation Analysis," Fusion Technology, 19, 1837 (1991).

9. E. Browne and R. Firestone, "Table of Radioactive Isotopes," Jone Wiely and Sons (1986).

6.8.5.3 Accident Analysis

First Wall and Blanket Thermal Response Under Loss-of-Cooling Accident – The temperature responses of the SiC first wall and blanket components under a loss of coolant accident are estimated in this section. It is assumed that the reactor can be shut down immediately after an accident occurs. The decay heat histories after reactor shutdown for various components are calculated assuming two full power years of operation. Results are shown in Figure 6.8.5-15. At the time of shutdown, the specific decay heat at the SiC first wall is about 0.6 W/cm^3 and drops to about 0.03 W/cm^3 at 10 minutes after shutdown. The specific decay heat of the lead coolant does not change significantly in the first 24 hours after shutdown.

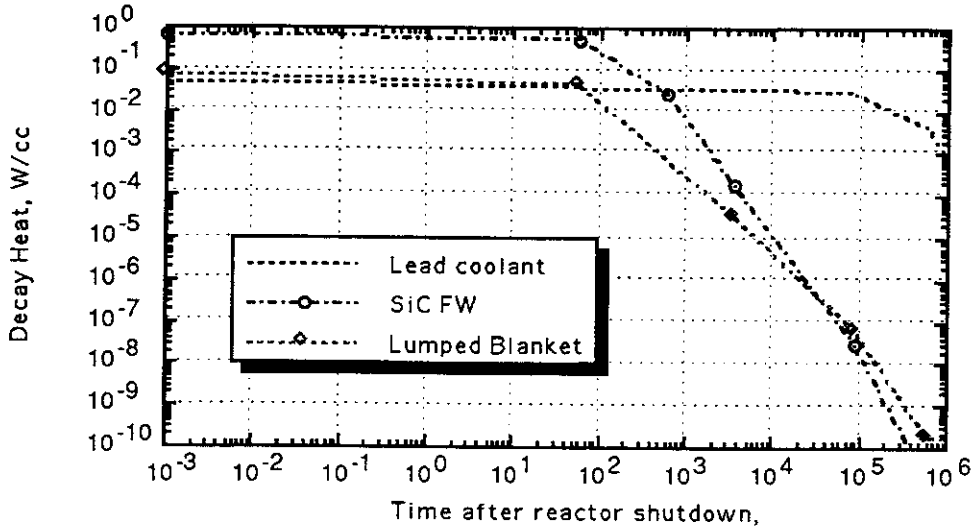

Figure 6.8.5-15. Specific Decay Heat Histories at Different Components

The component temperature history under adiabatic heatup with insulated boundaries can be estimated as:

$$\rho C_p \frac{\partial T}{\partial t} = q''' \qquad (6.8.5.3\text{-}1)$$

The assumption of adiabatic heatup with insulated boundaries is very conservative since in reality all the surrounding structures will also warm up. Figure 6.8.5-16 shows the temperature history of the SiC FW following a LOCA. The temperature of the SiC reaches about 445°C at 24 hours following reactor shutdown and stays quite flat for the following time.

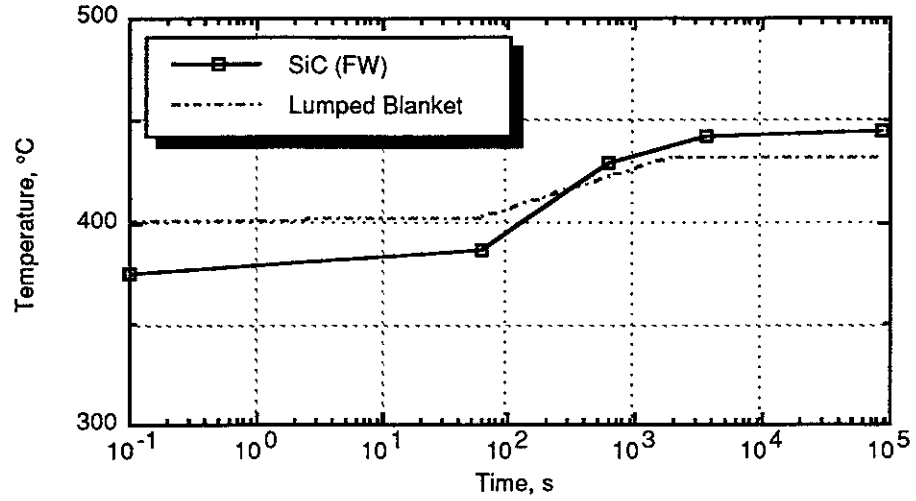

Figure 6.8.5-16. Temperature Histories at SiC FW and Blanket Components Following a Loss of Coolant Accident

As shown in Figure 6.8.5-15, the specific decay heat in the blanket is lower compared to that of the first wall structure. The lumped blanket temperature history under a LOCA with reactor shutdown is also shown in Figure 6.8.5-16. The results indicate that the temperature rise in the blanket module is about 35°C at one day following a loss of coolant accident.

Lead Decay Heat Removal Under Accident Conditions – Decay heat coming from radioactive lead poses a safety concern if it is not removed adequately following the reactor shutdown. Under normal plant shutdown, the decay heat can be removed by circulating the lead to the heat exchanger for about one week before it is transferred to the hot cell. However, under some off-normal conditions, additional heat removal mechanisms are required to remove the decay heat. Some of these scenarios include: (1) the lead spreads over the floor following a loss-of-coolant accident, (2) the lead becomes stagnant in the reactor due to failures of cooling pumps, or (3) a loss of heat sink (beyond the heat exchanger).

It is assumed that the plant design provides gravity-driven guided coolant drain paths. In this case, the lead can be collected in a pre-defined storage container and active cooling is suggested for the normal decay heat transport mechanism. In Prometheus, we go one step further to ensure that the decay heat can be removed passively, even in the event that all active cooling systems are lost.

There are four stages of heat removal which need to be considered: source term, transport pathways, intermediate heat storage, and ultimate heat sink. The source

term has been obtained from radioactivity calculations and is shown in Figure 6.8.5-15. After one week, the decay heat drops rapidly and the need for further heat rejection is essentially eliminated.

Several intermediate and ultimate heat sinks are available, including: (1) the earth beneath the reactor building, (2) the air surrounding the reactor building, (3) existing components within the reactor building, and (4) engineered safety system for heat storage.

Four different passive heat removal mechanisms have been explored here. These include:

(1) Heat of vaporization.
(2) Heat of fusion.
(3) Heat storage in solids and conducting to the earth.
(4) Heat storage in solids and convecting to the air.

The advantages and disadvantages of each concept is summarized in Table 6.8.5-7 and described in more detail below. Heat of vaporization is the most effective heat removal mechanism. Heat removed by storing decay heat in solids and conducting to the earth is an attractive alternate method.

Table 6.8.5-7 Summary of Passive Lead Decay Heat Removal Systems

Concept	Advantage	Disadvantage
Heat of Vaporization	Simple in concept Simple operation High storage potential per mass	Large storage volume
Heat of Fusion	High energy storage potential per unit mass Least volume required	Heat stored inside the medium requires an additional heat removal mechanism; Material compatibility
Heat Stored in Solids	Simple in concept Simple operation	Large material volume; Additional heat removal mechanism (conduction or convection) required; Good thermal contact required between storage container and solid mass.

1. Heat of Vaporization - Water has a relatively high heat of vaporization (2.2569×10^6 J/kg @ 1 atm). Steam can be generated by conduction through the storage container and into a water enclosure. The non-radioactive steam generated is then diverted to the atmosphere, making this a very promising concept for lead decay heat removal. During the first day following the reactor shutdown, the amount of steam generated is about 0.5 kg/sec for a lead inventory of 30 m^3. The total amount of water vaporized during a one-week period is about 300 m^3. After one week following reactor shutdown, decay heat level drops about two orders of magnitude, at which time the amount of water vaporized becomes insignificant.

2. Heat of Fusion - This concept utilizes a molten salt with a melting point of approximately 627°C as the heat storage medium. The heat stored inside the molten salt can be conducted (and/or convected) out to the ultimate heat sink, such as earth or atmosphere, over a longer period of time without jeopardizing the structure material. The concept appears attractive because of the small volume of material needed to remove the lead decay heat. The heat of fusion of LiF-NaF eutectic is between 167 and 222 kcal/kg (about 8.4×10^5 J/kg). Calculations show that approximately 8×10^5 kg of this eutectic would be needed to transport the lead decay heat.

3. Storage in Solids and Conduction to the Earth Over a Longer Time Span - This concept involves a large iron liner beneath the reactor building and welded (or otherwise attached) to the lead storage container. Decay heat from the lead is transmitted to the liner and then dissipated by conduction to the earth. The material considered for heat storage and transmission is cast iron, which melts at 1810 K. The storage unit is to be located at the bottom level of the plant to minimize the possibility of radioactive lead migration. The volume required for a temperature rise of 300°C over a one-week period is about 600 m^3 for a lead inventory of 30 m^3. Further temperature rise of the iron storage unit is limited due to a significant drop of the decay heat level.

4. Storage in a Solid Mass and Transport to the Atmosphere Through Natural Convection of Air - This concept is similar to the previous one. However, in this case the storage unit must be located close to the reactor boundary for better heat removal by natural convection. In addition, since the convective heat transport rate increases with height, this concept requires much more vertical space (the example below assumes 30 m). The lead decay heat is transmitted to the heat storage unit (a solid mass such as cast iron) and convected to the air through natural convection. The average heat transfer coefficient for a flat vertical surface is given as:

$$h = 0.555\,(GrPr)^{0.25}\left(\frac{k}{L}\right) \text{ for laminar flow}$$

$$= 0.021\,(GrPr)^{0.4}\left(\frac{k}{L}\right) \text{ for turbulent flow}$$

where the Grashof number (Gr) is calculated as:

$$Gr = \frac{\rho^2 g\beta\,(T_s - T_a)\,L^3}{\mu^2}$$

T_S and T_a are the surface and ambient temperatures, respectively, and L is the vertical height. The calculations show that, for an average surface temperature of 300°C and a height of 30 m, a surface area of 215 m^2 is needed. The volume of a storage unit using cast iron is about 600 m^3 for a temperature increase of 300°C.

Dry Spot Analysis – The SiC first wall behavior resulting from the formation of local dry spots has been analyzed using the radiation model discussed in Section 6.8.2.5. The formation of local dry spots has serious consequences on the performance and the expected lifetime of the reactor. A dry spot on the chamber wall will lead to erosion of the SiC structure, which could lead to an unscheduled shutdown of the reactor for maintenance. If the formation of these dry spots occurs frequently in a specific area, i.e. on the upper end cap, the maintenance costs of the design could increase drastically, thus decreasing the design's attractiveness.

The possible causes and effects of a dry spot are shown in Figure 6.8.5-17. Four different events that could lead to a local dry spot have been identified: blockage of the SiC, poor wetting of the first wall by the lead, hydrodynamic fluid instabilities, and uncovering of the wall by a loss of flow accident.

The porous SiC could become blocked by impurities in the liquid lead or by sintering of the structure at high operating temperatures. Since it is uncertain how corrosive liquid lead is at the temperatures of interest, solid particulates of the first wall system and the coolant pipes could flake off into the lead. These particulates could then clog the pores of the first wall. The high temperature environment of the reactor chamber could, after prolonged exposure to these temperatures, lead to sintering of the porous structure. If this happens, the lead will be blocked from reaching the surface of the blast chamber.

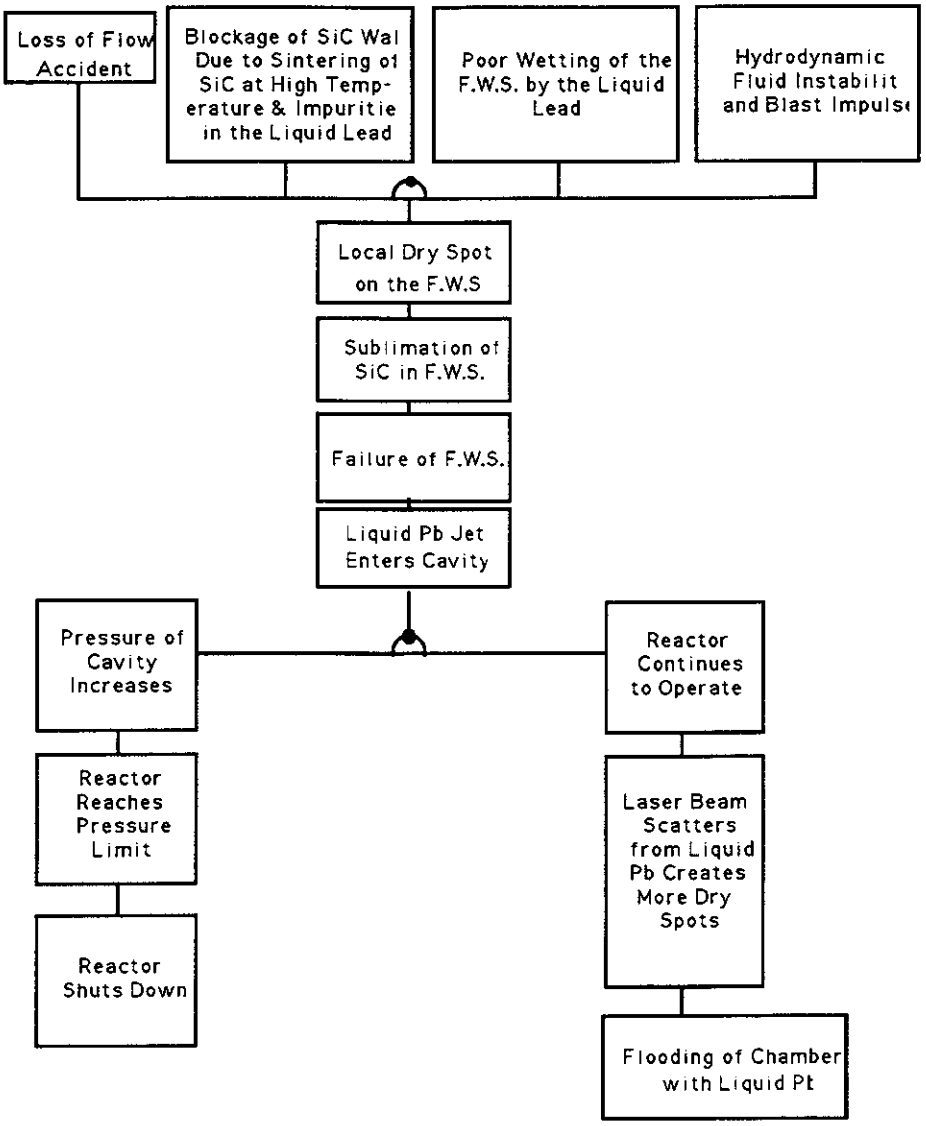

Figure 6.8.5-17 Scenarios of Dry Spot Formation Which Lead to a Reactor Shutdown.

Lead does not wet silicon carbide. Wetting agents are proposed to overcome this problem; however, the degree of wetting is still a concern. A heavy liquid film is very difficult to keep attached to an inverted surface even when the liquid wets the wall thoroughly. Along with the problem of wetting the inverted surface, the pressure waves created by a pellet explosion cause the wall to vibrate at frequencies of about 800 Hz. These vibrations can create instabilities in the liquid protectant causing the film to detach itself from the wall. The pressure wave can also cause the liquid lead to be pushed back far enough into the porous wall to prevent it from re-establishing itself on the surface in time for the next shot.

If, for any of the above reasons, a dry spot is established, the high heat fluxes that are generated after a blast will cause the exposed SiC to sublimate. The amount and thickness of the material that is evaporated can be estimated on a per shot basis and, from this, an estimate can be made of the time before the first wall fails. The radiative and conductive heat fluxes are shown in Figure 6.8.5-18. For very short times, ~10^{-14} s, the temperature gradient is large enough to conduct the energy out, but between 10^{-14} and 10^{-4} s the radiative flux dominates and an excess amount of energy can sublimate the SiC. The amount of energy per second per unit area that goes into evaporating the first wall is then:

$$E_{sub} = q_{rad} - q_{cond}$$

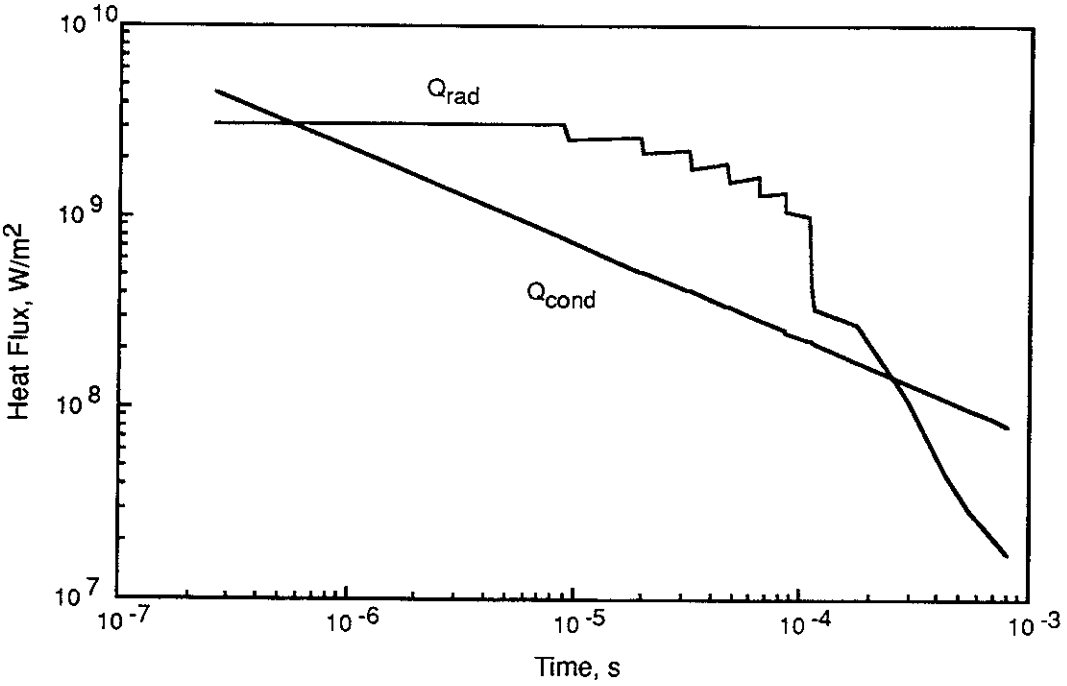

Figure 6.8.5-18. The Energy Available for Sublimation is the Difference Between the Radiative and Conductive Heat Fluxes.

The conductive heat flux is calculated by:

$$q_{cond} = k\frac{\Delta T}{\delta}$$

where δ is the thermal boundary layer thickness, which is defined as:

$$\delta = \sqrt{\pi \alpha t}$$

To calculate the amount of mass evaporated from the wall during a shot, E_{sub} is equated to the energy of sublimation, $H_{sub} = m\ h_{sub}$. The heat of sublimation is obtained from the potential energy of the Si and C atoms in the SiC matrix.[1] It is calculated to be:

$$h_{sub} = 1.91 \times 10^7, \text{ J/kg}$$

From this the mass of evaporated liquid per unit area can be calculated from:

$$m = \int_{t_o}^{t_m} \frac{E_{sub}}{h_{sub}}\, dt$$

From which the sublimation thickness is defined:

$$\Delta X = \frac{m}{\rho}$$

For the laser base case, the evaporation thickness per shot is calculated to be $\delta = 0.79\ \mu m$. The mean time to failure can be estimated as the time to sublime 5 mm of SiC, which equates to approximately 19 minutes of full power operation.

This calculation shows that the damage caused by a local dry spot needs to be managed. There must not be any prolonged dry spots on the first wall, thus making the stability of liquid film and detection of dry spots important issues.

Reference for 6.8.5.3

1. E. Pearson, T. Tadayoshi, T. Halicioglu, and W. Tiller, "Computer Modeling of Si and SiC Surfaces and Surface Process Relevant to Crystal Growth From the Vapor," Journal of Crystal Growth, 70, pp. 33-40 (1984).

6.8.5.4 Summary - The safety aspects of the Prometheus cavity have been addressed in this section. The analyses performed include radioactivity characterization and accident tolerances. The impacts of the resulted radioactive products and quantities from the cavity components on the environment are addressed in Section 6.13. Po^{210} is a safety concern when lead is chosen for the first wall coolant. The calculated Po^{210} inventory (due from bismuth impurity and bismuth generated from neutron interaction with lead) is one order of magnitude lower than the ESECOM Case 1 limiting case. It is concluded that the Prometheus design can be classified as LSA-1 with regards to Po^{210}.

To prevent lead coolant from spreading over the floor assuming a cooling tube rupture condition, the cavity is designed to allow the lead to be drained to a storage container through gravity-driven paths. In addition, several means of passive heat removal mechanisms have been explored. A passive safety feature with regards to lead decay heat removal under accident conditions can be met.

Formation of the dry spot on the first wall surface is considered unlikely. However, if the dry spot were sustained, the SiC structure could withstand 19 full-power minutes of operation before a failure of the FW would occur.

Based on all of the analysis performed, Prometheus is a very safe and environmentally attractive reactor concept.